Understanding the Adsorption Energetics of Growth Polymorphs of Ferrocene Derivatives: Microscopic Thermal Desorption Analysis

Prithwidip Saha,[†] Vivek Kumar Yadav,[‡] Vinithra Gurunarayanan,[†] Ramesh Ramapanicker,[†][ID] Jayant K. Singh,[‡][ID] and Thiruvancheril G. Gopakumar*,[†][ID]

[†]Department of Chemistry and [‡]Department of Chemical Engineering, Indian Institute of Technology Kanpur, Kanpur UP-208016, India

Ⓢ *Supporting Information*

ABSTRACT: The ultrathin films of 2-ferrocenyl-1,3-dithiolane (FcS_2C_3) and 2-ferrocenyl-1,3-dithiane (FcS_2C_4) drop-casted from toluene on highly oriented pyrolytic graphite (HOPG) surface are investigated using atomic force microscopy (AFM). Two types of growth polymorphs have been observed, which are distinctly different based on their nature of growth and the molecular level packing. We have developed a new type of temperature-dependent desorption experiment named "microscopic thermal desorption analysis" (MTDA) for understanding the adsorption energetics related to the observed growth polymorphs on the surface. Using MTDA, we have calculated the adsorption energies of growth polymorphs of both molecules and further revealed that their formation requires an activation energy. The subtle relation between the adsorption energies and activation energies of growth polymorphs account for their average abundance on the surface. The experimental observations are further supported by density functional theory (DFT) calculations.
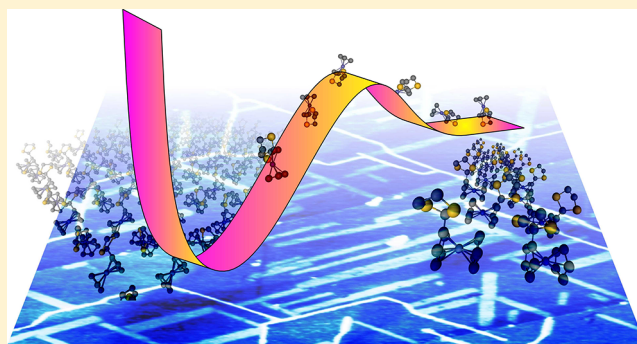
INTRODUCTION

Ferrocene (Fc), a sandwich transition metal complex of iron and cyclopentadienyl (Cp), is well-known for its controllable electronic and magnetic properties.[1−3] Because of the tunability of their electronic properties, thin films based on Fc and its derivatives have recently attracted interest in electronic devices like diodes, rectifiers, and transistors.[4−12] The control on the microscopic structure, in turn, is crucial in tuning their electronic properties. Fc derivatives with various functional groups have been used as a tool for controlling the microscopic structure of thin films under ultrahigh vacuum[1,13−26] and at ambient conditions.[27−32]

Recently, we have shown that solvents can be used as a control for tuning the microscopic pattern of thin films of Fc derivatives at ambient conditions.[33] In this article, we have studied the ultrathin films of 2-ferrocenyl-1,3-dithiolane (FcS_2C_3) and 2-ferrocenyl-1,3-dithiane (FcS_2C_4) drop-casted from toluene on highly oriented pyrolytic graphite (HOPG). An unusual long anisotropic growth (1D chain) is observed for both molecules when drop-casted from toluene, which is never observed when molecules are deposited from solvents like methanol, ethanol, dichloromethane, dimethylformamide, and acetone at ambient conditions. In addition to 1D chains, we observed another ordered assembly of molecules (1D island) which is ≈10 times more abundant than the 1D chain at ambient conditions. To understand the abundance and its relation to the adsorption energy of the growth polymorphs on

the surface, we have performed a new type of desorption experiment, namely "microscopic thermal desorption analysis" (MTDA). In MTDA, we measure the average abundance of different growth polymorphs at different annealing temperature using AFM micrographs. Using the average abundance and an equilibrium desorption−adsorption model, we determined the adsorption energies of different polymorphs. Conventionally temperature-programmed desorption (TPD) has been performed on physisorbed molecules on different surfaces[34−39] to understand their adsorption energies and phase transitions. TPD is a bulk measurement, and the averaging effect causes difficulties in differentiating the assemblies with a subtle difference in adsorption energy. Microscopy is therefore a possible alternative. We show that using MTDA, we can measure small differences in the adsorption energies of growth polymorphs of FcS_2C_3 and FcS_2C_4. The micrographs involved in every step reveal the overall microscopic nature of the surface, which is an added advantage of MTDA over TPD. We also note that using scannig tunneling microscopy (STM), at the solid−liquid interface, temperature-controlled desorption kinetics has been demonstrated previously.[40]
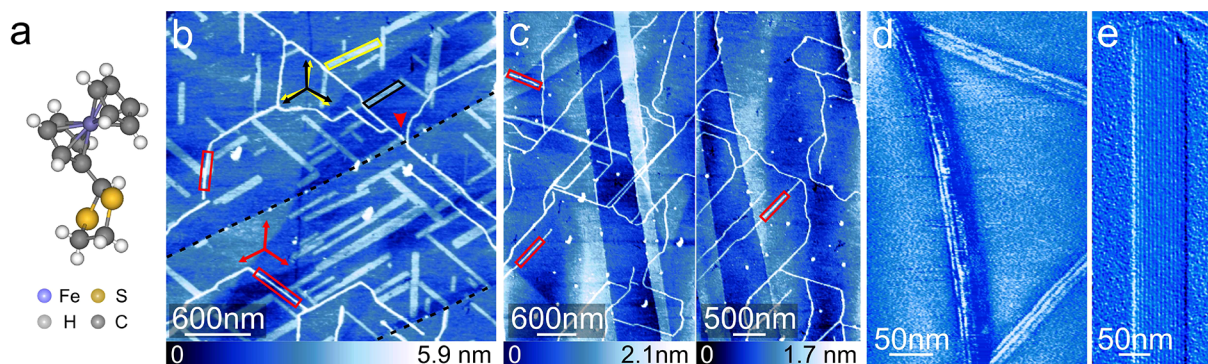
Figure 1. (a) Ball and stick model of FcS_2C_3 obtained from X-ray crystallographic data. (b) AFM topograph of an ultrathin film of FcS_2C_3 on HOPG (0001) surface deposited from toluene. Two types of molecular domains are observed and are named 1D island (yellow and black lines) and 1D chain (red lines). Rotational domains of 1D islands are marked with yellow and black arrows, whereas for the 1D chain, it is marked with red arrows. The growth of the 1D chain which crosses through the terrace edge is marked with a red arrowhead. Few terrace edges are indicated with black dashed lines. (c) Large area topographs of an area showing exclusively 1D chains. High-resolution phase image of a few 1D chains (d) and amplitude image of a 1D island (e).

EXPERIMENTAL DETAILS

Surface characterization is performed using an Agilent 5500 atomic force microscope (AFM) in intermittent contact mode. Aluminum-coated silicon cantilevers from Nanosensors (PPP-NCHR) are used as AFM probes. The resonance frequency and the spring constant of the cantilever are ≈300 kHz and 30−34 N/m, respectively. Image processing is performed using WSxM application from Nanotec. The drop-casting method is employed to produce the ultrathin films of molecules from solution phase (concentration ≈ 10^{-5}–10^{-6} M) on freshly cleaved HOPG (ZYB grade from μmasch). 3−4 μL of the solutions of FcS_2C_3 and FcS_2C_4 (in AR grade (>99.9%) toluene/methanol) are drop-casted on HOPG, keeping the surface at ≈20°−30° to ensure a smooth flow and uniform spreading of the solution over the substrate. It is then dried in ambient conditions for ≈5 min followed by mild pumping (0.01 mbar) for complete removal of the solvents, and surface imaging is performed afterward. Annealing of the solid state film is executed on hot plate at ambient conditions. While annealing, the temperature of the HOPG surface is measured with a K-type thermocouple with a typical error of ≈0.4−0.7 °C. For the annealing experiments; the surface is kept at ≈45 min at elevated temperatures. We note that it takes approximately 3−4 min for the surface to reach the annealing temperature as obtained from control experiments. We have also performed additional experiments at longer time of heating and have not observed any distinguishable difference compared to annealing at 45 min. During AFM studies, the relative humidity (≈50%) and temperature (23−26 °C) of the room are maintained by an air conditioner and a dehumidifier. 2-ferrocenyl-1,3-dithiolane (FcS_2C_3) and 2-ferrocenyl-1,3-dithiane (FcS_2C_4) are synthesized according to the literature.[33,41] The chemical structures of the molecules are included in the Supporting Information.

RESULTS AND DISCUSSION

Figure 1a shows a ball and stick model of 2-ferrocenyl-1,3-dithiolane (FcS_2C_3) as obtained from the bulk X-ray crystal structure data. Figure 1b shows a typical AFM topograph of an ultrathin film of the molecule as deposited from toluene on HOPG (0001) surface at ambient conditions. The submonolayer coverage of FcS_2C_3 reveals molecular domains, which are typically appearing as bright contrasts on the surface (with respect to pristine HOPG (blue)). Two types of molecular domains are observed within the submonolayer coverage, which are distinguishable by their nature of growth. The first type is observed as long islands with well-defined edges, and their growth is limited to a few hundreds of nanometers (indicated using yellow and black lines). It is also observed that this type of island is confined within the given terraces. We term this type of growth as 1D islands. This growth was previously observed for FcS_2C_3 from different solvents.[33] In contrast, the other types of molecular domains are very long and grow up to a few micrometers (maximum length observed: ≈4 μm). Part of two such domains are marked with red lines, and we address this type of growth as 1D chains. Interestingly, the 1D chains grow over monatomic terraces uninterrupted (indicated by red arrowhead), and the growth is restricted only by other molecular domains. The average width and apparent height of the 1D chains are ≈25 nm and ≈2.5 nm, respectively, which make it distinctly distinguishable from 1D islands. Height profiles of 1D chains and 1D islands are shown in the Supporting Information. Figure 1c shows topographs of an area with ≈100% abundance of 1D chains (area with ≈100% abundance of 1D islands is included in the Supporting Information). To ensure that these long features are not originating from pure graphite or solvents, we have analyzed freshly cleaved HOPG with and without solvents at different temperatures. Images of HOPG surface after depositing pure solvents and at higher temperature are given in the Supporting Information.

High-resolution AFM phase image of a few 1D chains and amplitude image of a 1D island are provided in Figures 1d and 1e, respectively. Periodic line-like contrasts are revealed along the length of the island and chains. The average spacing between adjacent line-like features is 0.6 ± 0.1 and 0.8 ± 0.1 nm in 1D islands and 1D chains, respectively. It is to be noted that the spacing is much larger compared to the size of the molecule. Therefore, we suggest that the contrast is originating due to the moiré effect of molecular rows within the islands/chains. The moiré effect arises due to incommensurate adsorption of adjacent molecular rows with respect to the surface sites.[28,33] Interestingly, the line-like contrast runs along the entire length of islands/chains uninterrupted, which indicates that the 1D islands and 1D chains are monocrystalline in nature.
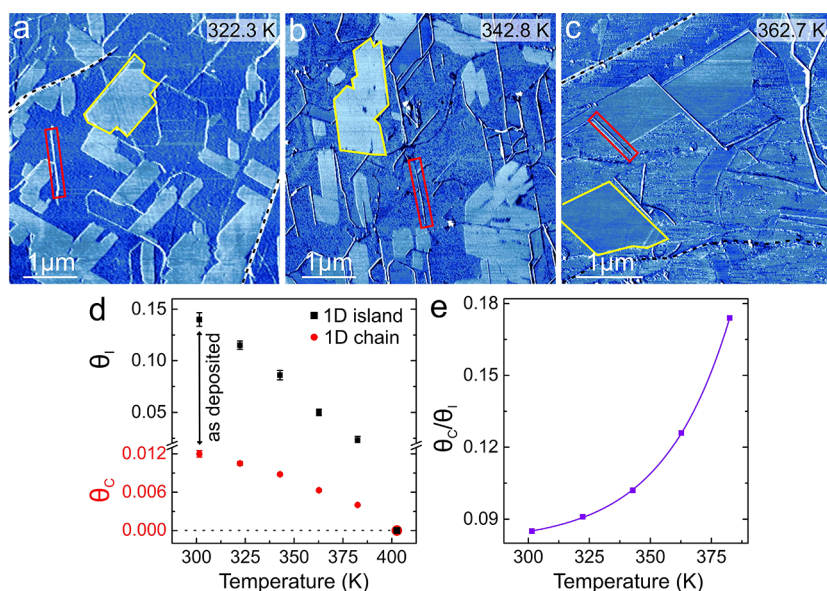
Figure 2. (a, b, c) AFM phase images of ultrathin films of FcS_2C_3 obtained after annealing the ambient prepared ultrathin film at ~322.3, ~342.8, and ~362.7 K, respectively. 1D islands are marked with yellow lines whereas 1D chains are marked with red lines. (d) Average abundance of 1D islands (black) and 1D chains (red) as a function of temperature. (e) Ratio of abundance of 1D chains and 1D islands (θ_C/θ_I) plotted as a function of temperature.

It is also observed that both 1D islands and 1D chains have preferred growth directions (referring to long edges). A statistical analysis (data provided in the Supporting Information) is performed for the angle between the long edges of 1D islands and is observed that there are six major orientations centered around ≈0/60/120° (marked by yellow and black arrows). On the other hand, the 1D chains show only three distinct growth directions (with respect to their long edge) at ≈0/60/120° (marked by red arrows). The orientations suggest that 1D islands are rotated by ±4° with respect to graphite compact directions and 1D chains are aligned to graphite compact directions. On the basis of the nature of the growth and the orientation of molecular rows with respect to graphite compact directions, it can be summarized that the microscopic pattern for 1D chains and 1D islands are different (will be discussed later).

The average abundance of the 1D islands and 1D chains is 0.140 ± 0.006 and 0.0120 ± 0.0005, respectively, obtained from statistical analysis (see details in the Supporting Information). On the basis of the average abundance, using Boltzmann statistics, it can be suggested that the formation of 1D islands are energetically preferred over 1D chains. In other words, the adsorption energy of 1D islands is larger compared to 1D chains. If this is true, then the ratio of average abundance of 1D chain to 1D island (θ_C/θ_I) should decrease as the temperature increases. To prove the above statement and to understand the adsorption energies of these growth polymorphs, we have performed a temperature-dependent abundance study of 1D chains and 1D islands on the surface. We term the method as "microscopic thermal desorption analysis" (MTDA).

In MTDA, we analyze the change in abundance of each polymorph as a function of temperature using the corresponding micrographs. Because we use micrographs to analyze the abundance, we have a microscopic understanding of the film and the polymorphs at different temperatures. Thus, the different types of polymorphs desorbing from the surface is accounted independently, and their adsorption energies are not averaged out. We perform the experiment as follows: the ultrathin film prepared from toluene at ambient conditions is subjected to annealing to a higher temperature at an interval of ≈20 K up to complete desorption of the film from the surface (≈410 K in this case). Figures 2a, 2b, and 2c show typical AFM phase images of ultrathin film of FcS_2C_3 after annealing to ~322.3, ~342.8, and ~362.7 K, respectively (images are obtained at RT). It is to be noted that the 1D islands coalesce (marked with yellow line), and therefore the average size of the islands appears larger compared to that at room temperature. We note that the orientations (with respect to long edge) of the islands are the same as that observed for 1D islands at room temperature (marked with yellow and black arrows). Unlike 1D islands, the 1D chains are observed as individual chains (a few chains are indicated with red lines) after heating. Therefore, we propose that the 1D chains do not coalesce with themselves or with 1D islands. Additional AFM phase images at various annealing temperatures are shown in the Supporting Information.

The average abundance obtained for 1D islands (θ_I) and 1D chains (θ_C) as a function of temperature is shown in Figure 2d. The first points (indicated using double-headed arrow) correspond to the abundance of 1D islands and 1D chains from the "as-deposited ultrathin film" from toluene. It is found that with increasing temperature, the abundance of both polymorphs decreases as expected. However, the ratio of the abundance of 1D chains to 1D islands (θ_C/θ_I) shows an unexpected increase as a function of the temperature (cf. Figure 2e). This suggests that the rate of desorption for 1D islands is higher than that of 1D chains.

We use the following model to understand the formation of different growth polymorphs. A suggestive free energy profile (q is intermolecular distance) for the adsorption/desorption process without activation barrier (blue dashed line) and with activation barrier (solid red/black lines) is shown in Figure 3a. If the adsorption/desorption is activation barrierless (blue dashed line, Figure 3a), then the adsorption energy (E_{ads}) is equal to the desorption energy (E_d). In this case, the
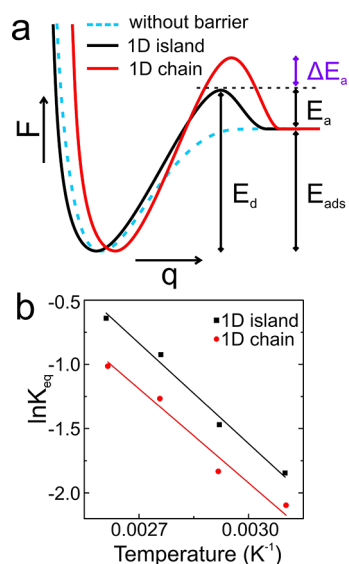
Figure 3. (a) Free energy profiles for the formation of molecular domains through different mechanisms. Black and red lines indicate the adsorption−desorption energy profile for the 1D island and the 1D chain, respectively. The dashed blue line indicates barrierless adsorption. (b) Calculated equilibrium constant K_{eq} as a function of inverse temperature for the 1D chain and 1D island.

polymorph with high E_{ads} will dominate the surface according to Boltzmann statistics (in the presence of no external influences). In addition, the ratio of the abundance of polymorphs (polymorph with low E_{ads} to high E_{ads}) will decrease with increasing temperature. On the contrary, if the adsorption requires an activation barrier (E_a), then E_{ads} is not equal to E_d (solid black/red lines in Figure 3a). E_a signifies that molecules are associatively adsorbing on the surface. If such a barrier exists for adsorption, then the abundance of different polymorphs on surface will be controlled by the height of E_a. Thus, the experimentally observed low abundance of 1D chain compared to the 1D island (as deposited) suggests the following possibilities: (a) barrierless adsorption with high E_{ads} for 1D islands compared to the 1D chain or (b) adsorption with activation barrier and the E_a for the formation of 1D chain higher compared to 1D islands. The increasing ratio of abundance of 1D chains and 1D islands (θ_C/θ_I) suggests that E_d is larger for the 1D chain than that of the 1D island. Thus, it can be concluded that the adsorption of both 1D chains and 1D islands possesses E_a, which is higher for the formation of the 1D chain compared to the 1D island.

Next, we quantify the E_{ads} for different polymorphs using the desorption experiment. Assuming that there is an equilibrium for the desorption of molecules from molecular domains to bare surface and eventually to the atmosphere at a given temperature. The activation barrier for the desorption of molecules from islands/chains to bare surface is E_d and that for re adsorption to islands/chains is E_a (cf. Figure 3a). If θ^i and θ^f are the initial and final abundance of the adsorbates in a given polymorph on the surface at a given temperature, then the equilibrium can be written as

$$\theta^i \underset{k_a}{\overset{k_d}{\rightleftharpoons}} \theta^f + [S]$$

where k_d and k_a are the rate constants of desorption and adsorption, respectively. [S] is the number of molecules that

desorb from the 1D islands or 1D chains and are available on the surface, which maintains the equilibrium. When the temperature increases, these free molecules evaporate from the surface, and new set of molecules desorb from 1D islands or 1D chains. Thus, eventually the overall abundance of the 1D chains and 1D islands is decreasing with increasing temperature. θ^i and θ^f of a given polymorph are obtained as follows. For example, the abundance of any polymorph at ∼301.5 K is equal to θ^i, and the abundance of that polymorph at ∼322.3 K is θ^f. The equilibrium constant of the desorption−adsorption process can be obtained according to Langmuir adsorption isotherm as follows.

$$K_{eq} = \frac{(1 - \theta^f)(\theta^i - \theta^f)}{\theta^i} \tag{1}$$

where K_{eq} is the equilibrium constant (k_d/k_a) of the desorption−adsorption process. The derivation of eq 1 is provided in the Supporting Information. K_{eq} can also be written in terms of E_d and E_a as follows (see details in the Supporting Information)

$$K_{eq} = A \exp\left(-\frac{E_d - E_a}{RT}\right) \tag{2}$$

$E_d - E_a$ is equal to E_{ads} of a given polymorph according to the desorption−adsorption free energy profile (cf. Figure 3a).

Using eq 1, we obtained K_{eq} for 1D chains and 1D islands at different temperatures. Figure 3b shows a plot of $\ln(K_{eq})$ as a function of $1/T$ (red dots and black squares). We employed eq 2 to obtain the adsorption energy for both types of polymorphs. The E_{ads} values obtained from the fitting (depicted by black/red lines in Figure 3b) for the 1D island (224.0 ± 0.9 meV) and the 1D chain (209.0 ± 1.3 meV) are comparable. The magnitude of the adsorption energy suggests that the intermolecular interactions are weak and of van der Waals origin. It is known for Fc-based molecules that the intermolecular interaction is a weak −C−H⋯π type interaction.[42−44] We also used θ_C/θ_I as a function of temperature to obtain the difference in E_a of the 1D chain and 1D island using Boltzmann statistics $(\theta_C/\theta_I = e^{-\Delta E_a/K_B T})$. The average difference in E_a of the 1D chain and 1D island is 63.6 meV (ΔE_a, cf. Figure 3a). This is well above the thermal energy at room temperature. Thus, it can be concluded that the E_{ads} of both 1D chains and 1D islands are comparable, and the observed low abundance of 1D chains at different temperatures is related to the high E_a of 1D chains compared to that of 1D islands.

To further validate the formation of different growth polymorphs, we have deposited FcS_2C_3 on HOPG from methanol at room temperature. Surprisingly, we did not observe 1D chains; instead, the surface is covered by monocrystalline 1D islands and polycrystalline 2D islands as reported previously.[33] AFM images and a description about the polymorphs are provided in the Supporting Information. The formation of different polymorphs in the ultrathin films (solid−air interface) of ferrocene derivatives has been reported previously. The selection of polymorphs on the surface depends on the boiling point of the solvents, with energetically favorable polymorphs being preferred on graphite when dropcasted from high boiling point solvents.[33] We note that solvent-induced polymorphsm is also known at the solid−liquid interface.[45,46] Upon annealing the ultrathin film, we observed 1D chains, which indicate that the 1D chains are a thermodynamically stable assembly of FcS_2C_3. As predicted by

the MTDA, the high adsorption barrier (E_a) of the 1D chain compared to the 1D island limits their formation at ambient temperature. However, it is interesting to note that the 1D chains are formed from toluene at room temperature. This is related to the selection of thermodynamically stable polymorphs by solvents with high boiling point as shown before[33]; see the discussion in the Supporting Information.

Next, we understand the molecular level assembly of 1D islands and 1D chains. The packing of molecules within the 1D islands has been microscopically understood in our previous work.[33] We have further optimized the geometry of previously proposed molecular packing in 1D islands on two-layer graphite using first-principles DFT as implemented in the Quantum ESPRESSO. Details of the calculations are included in Supporting Information. Figure 4a depicts the optimized
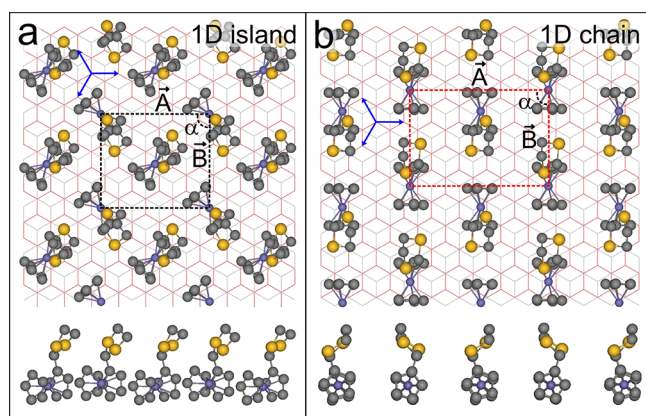
Figure 4. (a, b) Proposed models for molecular arrangement of FcS_2C_3 on the surface for the 1D island and the 1D chain, respectively. Corresponding side views are shown at the bottom. Unit cells of adlayers are marked with black/red dashed lines. $\vec{A}$ and $\vec{B}$ are the lattice vectors and α is the angle between these vectors. Blue arrows correspond to graphite compact directions.

molecular layer on graphite with unit cell marked by black dashed square. The lattice parameters of the adlayer are $\vec{A}$ = 0.984 nm, $\vec{B}$ = 0.850 nm, and α = 90°. The lower panel of Figure 4a shows the side view of the layer. The molecules within the assembly interact via an edge-to-face ($-C-H\cdots\pi$) interaction similar to that observed previously for other Fc derivatives.[42,44,47]

Unlike 1D islands, we were unable to obtain high-resolution images (both AFM/STM) due to the instability of the chains during the scanning. Therefore, we propose the packing for the 1D chain based on the literature and theoretical calculations. The optimized geometry (using first-principles DFT) of the proposed molecular arrangement (top and side view) on bilayer graphite is shown in Figure 4b. The building block of this assembly is different from that of the 1D island (see the unit cell marked with a dashed rectangle and the arrangement of adjacent molecules). The lattice parameters of the unit cell are $\vec{A}$ = 1.229 nm, $\vec{B}$ = 0.850 nm, and α = 90°. The adsorption geometry allows an edge-to-center ($-C-H\cdots$metal) interaction between adjacent molecules. This interaction is known as pregostic interaction,[48−50] which is also observed for assemblies of metallocenes.[29,43,44] Along $\vec{A}$, the Cp rings of the molecules are aligned to one of the graphite compact directions, which allows T-shaped $\pi-\pi$ (edge-to-face) interaction between Cp rings and graphite.[32,43,51,52] That is,

three equivalent adsorptions of the molecules are possible, and therefore three typical orientations are expected for 1D chains on graphite, which is in accordance with the experimental observation. The stability of the 1D islands and 1D chains may be compared from the calculated binding energies (BE; see details in the Supporting Information), which are −0.97 eV for the 1D island and −0.81 eV for the 1D chain for the proposed unit cell. We note that the BE is dependent on the size of the unit cell. The experimentally (MTDA) observed adsorption energies of 1D islands and 1D chains are lower than that obtained from the calculations. The BE obtained from DFT calculations (performed at 0 K) is not directly comparable to the adsorption energies obtained from experiments performed at higher temperatures. Because the molecules are thermally excited, it would not require the same amount of energy to desorb compared to a case when the molecules are at 0 K. However, on a relative scale, the calculations and experiments reveal that the BE/adsorption energy of molecules in 1D chains and 1D islands are comparable.

We performed desorption experiments on an ultrathin film of a slightly different molecule named 2-ferrocenyl-1,3-dithiane (FcS_2C_4). AFM images of ultrathin films of FcS_2C_4 annealed at different temperatures are provided in the Supporting Information. "As-deposited" films show 1D chains and 1D islands with a relatively high abundance of 1D islands. Upon annealing, the average abundance of both 1D chains and 1D islands reduces similarly as in FcS_2C_3. To obtain the adsorption energies of these polymorphs, we follow the same procedure as developed for the first case. Corresponding plots and detailed discussions are provided in the Supporting Information. It is found that the adsorption energy of the 1D island (289.0 ± 0.7 meV) is higher than that of the 1D chain (238.0 ± 0.7 meV). The theoretical calculations also show that the binding energy of 1D islands is higher than that of 1D chains. Optimized geometries corresponding to the 1D island and the 1D chain are given in the Supporting Information. It is also observed that E_a of 1D chains is higher than that of 1D islands, which is obtained from θ_C/θ_I, and ΔE_a is 76.2 meV. Thus, it is summarized that the relatively high abundance of 1D islands with respect to 1D chains is due to the contributions from both high E_{ads} of 1D islands and high E_a of 1D chains. It is also interesting to note that the average abundance of 1D islands of FcS_2C_4 (0.192 ± 0.004) is higher than that of 1D islands of FcS_2C_3 (0.140 ± 0.006). This presumably is due to the high adsorption energy contribution in the formation of 1D islands of FcS_2C_4.

■ CONCLUSION

We have investigated ultrathin films of 2-ferrocenyl-1,3-dithiolane and 2-ferrocenyl-1,3-dithiane drop-casted from toluene on HOPG at ambient conditions. Different types of growth polymorphs are observed; by use of AFM and theoretical calculations, the microscopic patterns of these polymorphs are understood. We have used a new method, which we name "microscopic thermal desorption analysis" (MTDA), for understanding the desorption energetics of growth polymorphs of these molecules on the surface. This method uses a combination of statistical analysis of the abundance of polymorphs and microscopy. Because MTDA uses microscopic images for the abundance of the growth polymorphs and addresses them separately, the obtained adsorption energies do not suffer from the averaging effect. Using MTDA, we show quantitatively various aspects of the

adsorption energetics for the growth polymorphs of FcS_2C_3 and FcS_2C_4 on graphite. This method may be extended to other molecular adsorbates on surfaces and will be used in understanding and fine-tuning molecular assemblies.

■ ASSOCIATED CONTENT

Ⓢ Supporting Information

The Supporting Information is available free of charge on the ACS Publications website at DOI: 10.1021/acs.jpcc.9b05557.

Chemical structures of FcS_2C_3 and FcS_2C_4; calculation of abundance of polymorphs; height profile of 1D chain and 1D island; AFM images of HOPG surface after depositing toluene and methanol solvents at different temperatures; areas with high abundance of 1D islands and 1D chains of FcS_2C_3; surface coverage of ultrathin film of FcS_2C_3 as a function of temperature; derivation of equilibrium constant K_{eq}; ultrathin film of FcS_2C_3 drop-casted from methanol; details of the theoretical calculations; and microscopic thermal desorption analysis (MTDA) for the ultrathin film of FcS_2C_4 (PDF)

■ AUTHOR INFORMATION

Corresponding Author

*E-mail: gopan@iitk.ac.in. Phone: +91 5122596830. Fax: +91 5122596806.

ORCID ⊙

Ramesh Ramapanicker: 0000-0002-7717-6843
Jayant K. Singh: 0000-0001-8056-2115
Thiruvancheril G. Gopakumar: 0000-0002-3219-7907

Notes

The authors declare no competing financial interest.

■ ACKNOWLEDGMENTS

■ REFERENCES

(1) Heinrich, B. W.; Limot, L.; Rastei, M. V.; Iacovita, C.; Bucher, J. P.; Djimbi, D. M.; Massobrio, C.; Boero, M. Dispersion and localization of electronic states at a ferrocene/Cu(111) interface. *Phys. Rev. Lett.* **2011**, *107*, 216801.

(2) Ormaza, M.; Robles, R.; Bachellier, N.; Abufager, P.; Lorente, N.; Limot, L. On-surface engineering of a magnetic organometallic nanowire. *Nano Lett.* **2016**, *16*, 588.

(3) Zhang, Y.; Deng, M. Electrical control of spin states of ferrocene on Cu(111). *J. Phys. Chem. C* **2015**, *119*, 21681.

(4) Fabre, B. Ferrocene-terminated monolayers covalently bound to hydrogen-terminated silicon surfaces. Toward the development of charge storage and communication devices. *Acc. Chem. Res.* **2010**, *43*, 1509.

(5) Li, Z.; Liu, Y.; Mertens, S. F. L.; Pobelov, I. V.; Wandlowski, T. From redox gating to quantized charging. *J. Am. Chem. Soc.* **2010**, *132*, 8187.

(6) Halik, M.; Hirsch, A. The potential of molecular self-assembled monolayers in organic electronic devices. *Adv. Mater.* **2011**, *23*, 2689.

(7) Mentovich, E. D.; Rosenberg-Shraga, N.; Kalifa, I.; Gozin, M.; Mujica, V.; Hansen, T.; Richter, S. Gated-controlled rectification of a self-assembled monolayer-based transistor. *J. Phys. Chem. C* **2013**, *117*, 8468.

(8) Nerngchamnong, N.; Yuan, L.; Qi, D.-C.; Li, J.; Thompson, D.; Nijhuis, C. A. The role of Van der waals forces in the performance of molecular diodes. *Nat. Nanotechnol.* **2013**, *8*, 113.

(9) Liu, J.; Wachter, T.; Irmler, A.; Weidler, P. G.; Gliemann, H.; Pauly, F.; Mugnaini, V.; Zharnikov, M.; Wöll, C. Electric transport properties of surface-anchored metal organic frameworks and the effect of ferrocene loading. *ACS Appl. Mater. Interfaces* **2015**, *7*, 9824.

(10) Yuan, L.; Nerngchamnong, N.; Cao, L.; Hamoudi, H.; del Barco, E.; Roemer, M.; Sriramula, R. K.; Thompson, D.; Nijhuis, C. A. Controlling the direction of rectification in a molecular diode. *Nat. Commun.* **2015**, *6*, 6324.

(11) Choi, J.-W.; Jung, G.-Y.; Oh, S. Y.; Lee, W. H.; Shin, D. M. Photoinduced electron transfer in a MIM device composed of TCNQ-pyrene-ferrocene LB films. *Thin Solid Films* **1996**, *284*, 876.

(12) Xiang, J.; Wang, T.-K.; Zhao, Q.; Huang, W.; Ho, C.-L.; Wong, W.-Y. Ferrocene-containing poly(fluorenylethynylene)s for non-volatile resistive memory devices. *J. Mater. Chem. C* **2016**, *4*, 921.

(13) Berger, J.; Kośmider, K.; Stetsovych, O.; Vondráček, M.; Hapala, P.; Spadafora, E. J.; Švec, M.; Jelínek, P. Study of ferrocene dicarboxylic acid on substrates of varying chemical activity. *J. Phys. Chem. C* **2016**, *120*, 21955.

(14) Wasio, N. A.; Quardokus, R. C.; Forrest, R. P.; Lent, C. S.; Corcelli, S. A.; Christie, J. A.; Henderson, K. W.; Kandel, S. A. Self-assembly of hydrogen-bonded two-dimensional quasicrystals. *Nature* **2014**, *507*, 86.

(15) Braun, K.-F.; Iancu, V.; Pertaya, N.; Rieder, K.-H.; Hla, S.-W. Decompositional incommensurate growth of ferrocene molecules on a Au(111) surface. *Phys. Rev. Lett.* **2006**, *96*, 246102.

(16) Quardokus, R. C.; Wasio, N. A.; Forrest, R. P.; Lent, C. S.; Corcelli, S. A.; Christie, J. A.; Henderson, K. W.; Alex Kandel, S. Adsorption of diferrocenylacetylene on Au(111) studied by scanning tunneling microscopy. *Phys. Chem. Chem. Phys.* **2013**, *15*, 6973.

(17) Tegenkamp, C.; Schmeidel, J.; Pfnür, H. Chemisorption of ferrocene on Si(111)−Ag√3: frustrated conformational flexibility. *Surf. Sci.* **2011**, *605*, 267.

(18) Zhong, D.; Wedeking, K.; Blömker, T.; Erker, G.; Fuchs, H.; Chi, L. Multilevel supramolecular architectures self-assembled on metal surfaces. *ACS Nano* **2010**, *4*, 1997.

(19) Zhong, D. Y.; Wang, W. C.; Dou, R. F.; Wedeking, K.; Erker, G.; Chi, L. F.; Fuchs, H. Oligoethylene-bridged diferrocene on Ag(110): monolayer structures and adsorbate-induced faceting. *Phys. Rev. B: Condens. Matter Mater. Phys.* **2007**, *76*, 205428.

(20) Nerngchamnong, N.; Wu, H.; Sotthewes, K.; Yuan, L.; Cao, L.; Roemer, M.; Lu, J.; Loh, K. P.; Troadec, C.; Zandvliet, H. J. W.; et al. Supramolecular structure of self-assembled monolayers of ferrocenyl terminated n-alkanethiolates on gold surfaces. *Langmuir* **2014**, *30*, 13447.

(21) Paul, R.; Reifenberger, R. G.; Fisher, T. S.; Zemlyanov, D. Y. Atomic layer deposition of FeO on Pt(111) by ferrocene adsorption and oxidation. *Chem. Mater.* **2015**, *27*, 5915.

(22) Ormaza, M.; Abufager, P.; Bachellier, N.; Robles, R.; Verot, M.; Le Bahers, T.; Bocquet, M.-L.; Lorente, N.; Limot, L. Assembly of ferrocene molecules on metal surfaces revisited. *J. Phys. Chem. Lett.* **2015**, *6*, 395.

(23) Brown, R. D.; Coman, J. M.; Christie, J. A.; Forrest, R. P.; Lent, C. S.; Corcelli, S. A.; Henderson, K. W.; Kandel, S. A. Evolution of metastable clusters into ordered structures for 1,1-ferrocenedicarboxylic acid on the Au(111) surface. *J. Phys. Chem. C* **2017**, *121*, 6191.

(24) Quardokus, R. C.; Wasio, N. A.; Christie, J. A.; Henderson, K. W.; Forrest, R. P.; Lent, C. S.; Corcelli, S. A.; Alex Kandel, S. Hydrogen-bonded clusters of ferrocenecarboxylic acid on Au(111). *Chem. Commun.* **2014**, *50*, 10229.

(25) Müller-Meskamp, L.; Karthäuser, S.; Waser, R.; Homberger, M.; Wang, Y.; Englert, U.; Simon, U. Structural ordering of

ferrocenylalkanethiol monolayers on Au(111) studied by scanning tunneling microscopy. *Surf. Sci.* **2009**, *603*, 716.

(26) Quardokus, R. C.; Wasio, N. A.; Brown, R. D.; Christie, J. A.; Henderson, K. W.; Forrest, R. P.; Lent, C. S.; Corcelli, S. A.; Alex Kandel, S. Hydrogen-bonded clusters of 1, 1-ferrocenedicarboxylic acid on Au(111) are initially formed in solution. *J. Chem. Phys.* **2015**, *142*, 101927.

(27) Muller-Meskamp, L.; Karthauser, S.; Waser, R.; Homberger, M.; Simon, U. Striped phase of mercaptoalkylferrocenes on Au(111) with a potential for nanoscale surface patterning. *Langmuir* **2008**, *24*, 4577.

(28) Saha, P.; Yadav, K.; Chacko, S.; Philip, A. T.; Ramapanicker, R.; Gopakumar, T. G. Controlling growth to one dimension in nanoislands of ferrocene-sugar derivatives. *J. Phys. Chem. C* **2016**, *120*, 9223.

(29) Wedeking, K.; Mu, Z.; Kehr, G.; Fröhlich, R.; Erker, G.; Chi, L.; Fuchs, H. Tetradecyl ferrocene: ordered molecular array of an organometallic amphiphile in the crystal and in a two-dimensional assembled structure on a surface. *Langmuir* **2006**, *22*, 3161.

(30) Yokota, Y.; Fukui, K.-I.; Enoki, T.; Hara, M. Origin of current enhancement through a ferrocenylundecanethiol island embedded in alkanethiol SAMs by using electrochemical potential control. *J. Phys. Chem. C* **2007**, *111*, 7561.

(31) Dou, R. F.; Zhong, D. Y.; Wang, W. C.; Wedeking, K.; Erker, G.; Chi, L.; Fuchs, H. Structures and stability of ferrocene derivative monolayers on Ag(110): scanning tunneling microscopy study. *J. Phys. Chem. C* **2007**, *111*, 12139.

(32) Qune, L. F. N. A.; Tamada, K.; Hara, M. Self-assembling properties of 11-ferrocenyl-1-undecanethiol on highly oriented pyrolitic graphite characterized by scanning tunneling microscopy. *e-J. Surf. Sci. Nanotechnol.* **2008**, *6*, 119.

(33) Saha, P.; Gurunarayanan, V.; Korolkov, V. V.; Vasudev, P. G.; Ramapanicker, R.; Beton, P. H.; Gopakumar, T. G. Selection of adlayer patterns of 1,3-dithia derivatives of ferrocene by the nature of the solvent. *J. Phys. Chem. C* **2018**, *122*, 19067.

(34) Kanjilal, A.; Ottaviano, L.; Di Castro, V.; Beccari, M.; Betti, M. G.; Mariani, C. Pentacene grown on self-assembled monolayer adsorption energy, interface dipole, and electronic properties. *J. Phys. Chem. C* **2007**, *111*, 286.

(35) Frank, P.; Djuric, T.; Koini, M.; Salzmann, I.; Rieger, R.; Müllen, K.; Resel, R.; Koch, N.; Winkler, A. Layer growth, thermal stability, and desorption behavior of hexaaza-triphenylene-hexacarbonitrile on Ag(111). *J. Phys. Chem. C* **2010**, *114*, 6650.

(36) Thrower, J. D.; Friis, E. E.; Skov, A. L.; Nilsson, L.; Andersen, M.; Ferrighi, L.; Jørgensen, B.; Baouche, S.; Balog, R.; Hammer, B.; et al. Interaction between coronene and graphite from temperature-programmed desorption and DFT-vdW calculations: importance of entropic effects and insights into graphite interlayer binding. *J. Phys. Chem. C* **2013**, *117*, 13520.

(37) Conti, S.; Cecchini, M. Accurate and efficient calculation of the desorption energy of small molecules from graphene. *J. Phys. Chem. C* **2015**, *119*, 1867.

(38) Thussing, S.; Jakob, P. Thermal stability and interlayer exchange processes in heterolayers of CuPc and PTCDA on Ag(111). *J. Phys. Chem. C* **2017**, *121*, 13680.

(39) Zhao, J.; Noffke, B. W.; Raghavachari, K.; Teplyakov, A. V. Temperature-programmed desorption (TPD) and density functional theory (DFT) study comparing the adsorption of ethyl halides on the Si(100) surface. *J. Phys. Chem. C* **2017**, *121*, 7208.

(40) Bhattarai, A.; Mazur, U.; Hipps, K. W. Desorption Kinetics and Activation Energy for Cobalt Octaethylporphyrin from Graphite at the Phenyloctane Solution-Graphite Interface: An STM Study. *J. Phys. Chem. C* **2015**, *119*, 9386.

(41) Philip, A. T.; Chacko, S.; Ramapanicker, R. Synthesis of stable C-linked ferrocenyl amino acids and their use in solution-phase peptide synthesis. *J. Pept. Sci.* **2015**, *21*, 887.

(42) Hartmann, S.; Winter, R. F.; Scheiring, T.; Wanner, M. Allylferrocenylselenide and the synthesis of the first seleno-substituted allenylidene complex: synthesis, spectroscopy, electrochemistry and the effect of electron transfer from the ferrocenylselenyl subunit. *J. Organomet. Chem.* **2001**, *637–639*, 240.

(43) Wedeking, K.; Mu, Z.; Kehr, G.; Cano Sierra, J.; Mück Lichtenfeld, C.; Grimme, S.; Erker, G.; Fröhlich, R.; Chi, L.; Wang, W.; et al. Oligoethylene chains terminated by ferrocenyl end groups: synthesis, structural properties, and two-dimensional self-assembly on surfaces. *Chem. - Eur. J.* **2006**, *12*, 1618.

(44) Bogdanović, G. A.; Novaković, S. B. Rigid ferrocene–ferrocene dimer as a common building block in the crystal structures of ferrocene derivatives. *CrystEngComm* **2011**, *13*, 6930.

(45) Mamdouh, W.; Uji-i, H.; Ladislaw, J. S.; Dulcey, A. E.; Percec, V.; De Schryver, F. C.; De Feyter, S. Solvent Controlled Self-Assembly at the Liquid-Solid Interface Revealed by STM. *J. Am. Chem. Soc.* **2006**, *128*, 317.

(46) Takami, T.; Mazur, U.; Hipps, K. Solvent-Induced Variations in Surface Structure of a 2,9,16,23-Tetra-tert-butyl-phthalocyanine on Graphite. *J. Phys. Chem. C* **2009**, *113*, 17479.

(47) Hitchcock, P. B.; Leigh, G.; Togrou, M. Lithiation of ferrocenylamines and vanadium dinitrogen chemistry. *J. Organomet. Chem.* **2002**, *664*, 245.

(48) Brookhart, M.; Green, M. L. Carbon—hydrogen-transition metal bonds. *J. Organomet. Chem.* **1983**, *250*, 395.

(49) Brookhart, M.; Green, M. L. H.; Parkin, G. Agostic interactions in transition metal compounds. *Proc. Natl. Acad. Sci. U. S. A.* **2007**, *104*, 6908.

(50) Pal, R.; Mebs, S.; Shi, M. W.; Jayatilaka, D.; Krzeszczakowska, J. M.; Malaspina, L. A.; Wiecko, M.; Luger, P.; Hesse, M.; Chen, Y.-S.; et al. Linear MgCp*2 vs bent CaCp*2: London dispersion, ligand-induced charge localizations, and pseudo-pregostic C—H···Ca interactions. *Inorg. Chem.* **2018**, *57*, 4906.

(51) Sinnokrot, M. O.; Valeev, E. F.; Sherrill, C. D. Estimates of the ab initio limit for $\pi-\pi$ interactions: the benzene dimer. *J. Am. Chem. Soc.* **2002**, *124*, 10887.

(52) Lee, E. C.; Hong, B. H.; Lee, J. Y.; Kim, J. C.; Kim, D.; Kim, Y.; Tarakeshwar, P.; Kim, K. S. Substituent effects on the edge-to-face aromatic interactions. *J. Am. Chem. Soc.* **2005**, *127*, 4530.